# Nanocrystalline TiO$_2$ Composite Films for the Photodegradation of Formaldehyde and Oxytetracycline under Visible Light Irradiation

**Min Wei [1], Xue-Lei Peng [2], Qi-Sheng Liu [1], Fang Li [1] and Ming-Ming Yao [1,*]**

[1]  Key Laboratory of Interfacial Reaction & Sensing Analysis in Universities of Shandong, School of Chemistry and Chemical Engineering, University of Jinan, Jinan 250022, China; emily518@foxmail.com (M.W.); chm_liuqs@ujn.edu.cn (Q.-S.L.); chm_lif@ujn.edu.cn (F.L.)

[2]  Jinan Institute of Product Quality Inspections, Jinan 250022, China; yaomm4364@sina.com

[*]  Correspondence: chm_yaomm@ujn.edu.cn; Tel.: +86-531-8276-5959; Fax: +86-531-8276-5969

**Abstract:** In order to effectively photodegradate organic pollutants, ZnO composite and Co-B codoped TiO$_2$ films were successfully deposited on glass substrates via a modified sol-gel method and a controllable dip-coating technique. Combining with UV–Vis diffuse reflectance spectroscopy (DRS) and photoluminescence spectra (PL) analyses, the multi-modification could not only extend the optical response of TiO$_2$ to visible light region but also decrease the recombination rate of electron-hole pairs. XRD results revealed that the multi-modified TiO$_2$ film had an anatase-brookite biphase heterostructure. FE-SEM results indicated that the multi-modified TiO$_2$ film without cracks was composed of smaller round-like nanoparticles compared to pure TiO$_2$. BET surface area results showed that the specific surface area of pure TiO$_2$ and the multi-modified TiO$_2$ sample was 47.8 and 115.8 m$^2$/g, respectively. By degradation of formaldehyde and oxytetracycline, experimental results showed that the multi-modified TiO$_2$ film had excellent photodegradation performance under visible light irradiation.

**Keywords:** TiO$_2$ film; multi-modification; photodegradation

## 1. Introduction

With industrialization and population growth, water pollution caused by recalcitrant organic compounds is becoming a major environmental problem [1]. In recent years, traditional physical and biological treatment methods—such as activated carbon adsorption, ultra-filtration, reverse osmosis, and coagulation—are used to remove the contaminants from wastewater. However, these techniques cannot transfer organic compounds into non-hazardous compounds [2]. Semiconductor heterogeneous photocatalysis, a new water treatment technology, is considered as an effective environmentally-friendly approach to decrease the concentrations of organic contaminants in various wastewaters [3]. Among various semiconductors, titanium dioxide is considered to be the most useful photocatalyst due to its physical and chemical stability, photo-corrosion resistance, non-toxicity, convenience of preparation, cost-effective breakdown of harmful organic molecules, etc. [4]. Powdered TiO$_2$ is limited as a photocatalyst since a post treatment separation is required to recover its photocatalysis in wastewater. Therefore, TiO$_2$ films coated on various substrates such as glass and ceramic tiles have attracted considerable interests recently [5].

According to our knowledge, anatase and rutile forms of TiO$_2$ have been investigated extensively as photocatalyst among the three common crystalline forms (anatase, brookite, and rutile), and antase-TiO$_2$ possess the best photocatalytic activity [6]. Since the light response range of pure TiO$_2$

is limited in the UV-light region, only photons with energies equal or greater than the band gap energy ($\Delta E \approx 3.2$ eV) can generate positive electrons ($e^-$) and holes ($h^+$) which then promote possible photocatalytic reactions [7]. When the generated charge carriers react with oxygen/water neighboring the photocatalyst, hydroxyl radicals with strong oxidation can be generated. In the light of these highly active radicals, the degradation process of organic pollutants can be easily caused in the air and water solution. This is the reason why $TiO_2$ can completely oxidize large quantities of aquatic organic pollutants to $CO_2$ and $H_2O$ through both oxidative degradation and reductive transformation. Unfortunately, the practical application of $TiO_2$ in photocatalysis is limited by its lower efficiency, which boils down to (i) an increase of the electron-hole pairs recombination rate i.e., a decrease of their lifetime; and (ii) the wide band-gap restricting light absorption to only ultraviolet region, thus limiting the range of light response to visible light region. To overcome the inherent weakness of $TiO_2$, numerous efforts have been made to increase its visible light absorption and prolong carrier's lifetime. Many popular techniques are used to modify $TiO_2$ including composite semiconductors, metal doping, and nonmetal doping [8,9].

Coupling with another semiconductor is regarded as a good method to improve the photocatalytic activity of $TiO_2$. Reportedly, ZnO is an excellent n-type semiconductor material exhibiting promising efficiency for photocatalytic oxidation of organic contamination. It is due to the intimate interfacial interaction between ZnO and $TiO_2$ via chemical bonding that ZnO can uniformly graft on the surface of $TiO_2$ to form the heterojunction. The mechanism for charge transfer in composite $TiO_2$-ZnO film can be graphically shown in Figure 1. The slight negative shift of the ZnO band facilitates the injection of electrons from the CB of ZnO to the CB of $TiO_2$, and the migration of holes from the VB of $TiO_2$ to the VB of ZnO upon illumination, which effectively increase the availability of $e^-$ and $h^+$ for targeted redox processes by reducing their recombination [10]. The technique may improve the photocatalytic performance of $TiO_2$ in a certain extent, but still cannot meet the actual needs. In order to effectively photodegrade organic pollutants, other modification methods also need to be used.
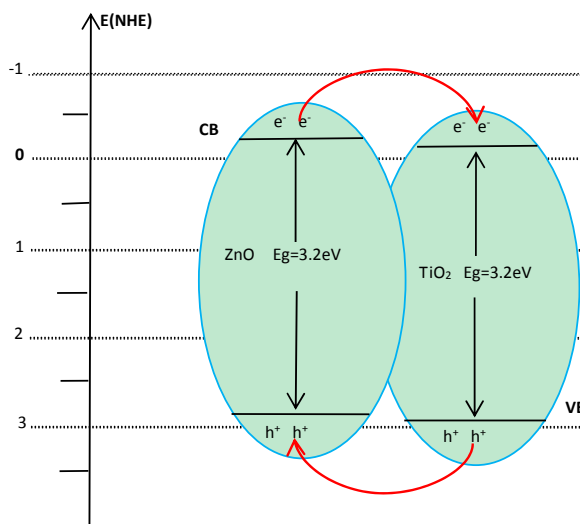


**Figure 1.** Schematic diagram for charge transfer in composite $TiO_2$/ZnO film.

Metal doping is another effective approach to modify $TiO_2$ films. It was commonly reported that Co doping can enhance the photocatalytic activity of $TiO_2$ due to narrowed band gap and diminished photo-generated electrons and holes combination [11], but difficulties involved in metal doping into $TiO_2$ are poor thermal stability during heat treatment, surface aggregation rather than substitution, and only a small red shift [12]. It is accepted that doping with nonmetal ions into a titania matrix provides favorable visible light response and facilitates efficient charge carrier transfer processes. B ions can be mainly incorporated into some metal oxide lattices in interstitial mode acting as shallow traps for

electrons to prolong the life of the photo-generated electrons and holes [13]. Normally, metal dopant energy levels are below the conduction band edge of $TiO_2$, while nonmetal dopant energy levels are just above the top of the valence band of $TiO_2$. This gives us a hint that low concentration codopants of metal and nonmetal ions may effectively narrow the band gap and enhance the visible light absorption efficiency. The aim of this study is to examine the effect of ZnO composite and Co-B codoping for $TiO_2$ photocatalysts on the photocatalytic degradation of oxytetracycline (OTC) and formaldehyde in an aqueous solution. It is expected that the multi-modified $TiO_2$ film can exhibit better photocatalytic properties due to the synergistic effect of two processes.

## 2. Experimental

### 2.1. Film Preparation

All reagents and chemicals were of analytical grade without any further purification and the water used was double-distilled deionized, invariably, in our experiment. Pure $TiO_2$, composite $TiO_2/ZnO$, Co doped $TiO_2/ZnO$, B doped $TiO_2/ZnO$, and Co-B codoped $TiO_2/ZnO$ films were prepared via applicable sol-gel technique employing tetrabutyl titanate ($Ti(C_4H_9O)_4$) and zinc acetate dihydrate ($Zn(CH_3COO)_2 \cdot 2H_2O$) as metal sources. The $TiO_2$ sol was prepared using tetrabutyl titanate, ethanol absolute (solvent), nitric acid (0.2 mol/L, catalyst) in a volume ratio of 1:20:20, correspondingly, in a clean and dry vessel at ambient temperature. The process was completed with vigorous stirring about 30 min till the homogeneous colloidal suspension was obtained, and the preparation procedure is described in detail in reference [14]. The ZnO sol was prepared as follows: the first step is to prepare $5 \times 10^{-3}$ mol/L zinc acetate ethanol solution, in which a certain amount of zinc acetate was dissolved in anhydrous ethanol under vigorous stirring. Then, in a volume ratio of 1:9, $2 \times 10^{-2}$ mol/L sodium hydroxide ethanol solution was added to the above solution dropwise with magnetic stirring for 30 min at room temperature. A transparent ZnO-sol was obtained after for two days [15]. The flow chart of $TiO_2/ZnO$ composite film preparation is shown in Figure 2.
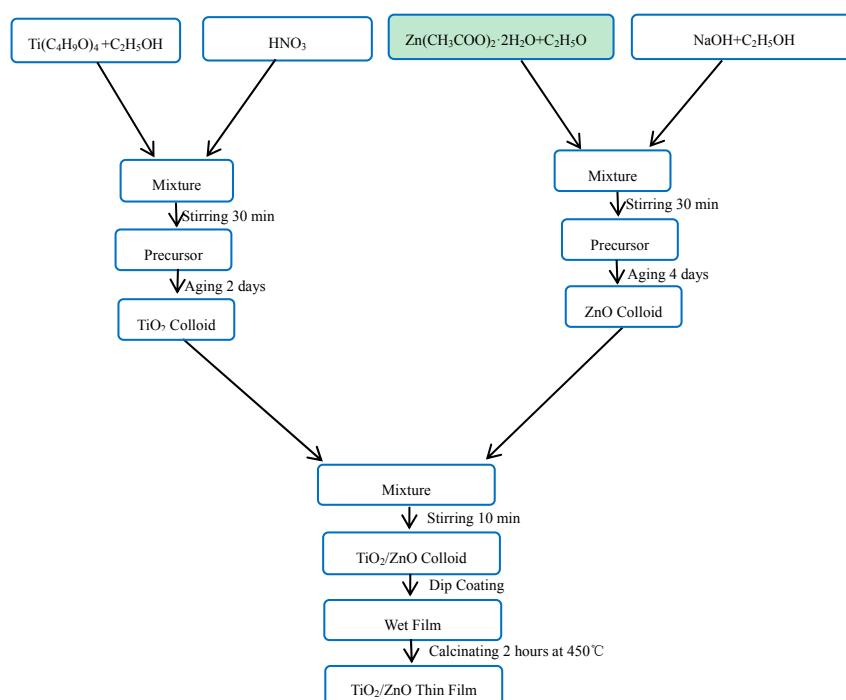


**Figure 2.** Flow chart of composite $TiO_2/ZnO$ film preparation.

The targeted films were immobilized to the surface of glass substrate ($25 \times 25 \times 1$ mm$^3$), which were cleaned by chromic acid lotion, and then rinsed by distilled water and ethanol, using a controllable dip-coating technique at ambient atmosphere. The speed withdrawal was maintained at 1 mm/s. TiO$_2$/ZnO composite films were prepared by repeating the deposition procedures of TiO$_2$ colloid and ZnO colloid, alternately. 0.1 mL $7 \times 10^{-3}$ M cobalt or 0.1 mL $9 \times 10^{-2}$ M boron ions were doped into the surface layer via coating cobaltous nitrate hexahydrate (Co(NO$_3$)$_2$·6H$_2$O) or boric acid (H$_3$BO$_3$) aqueous solution onto a dried TiO$_2$/ZnO composite film. At last, to remove organic substances contained in the gel and induce crystallization of particles, all as-prepared samples were calcined at 450 °C in a horizontal furnace for 1 h. In our experiments, the thickness of the films was 0.1–0.3 μm measured using a profilometer.

## 2.2. Catalyst Characterization

The UV–Vis diffuse reflectance spectra (DRS) of various films were recorded to analyze the light absorption via a UV–Vis spectrophotometer (TU-1901) equipped with an integrating sphere accessory (IS 19-1) using blank glass plate as a reference. In order to study the recombination of photo-generated electron-hole pairs in the Co-B codoped TiO$_2$/ZnO film, a FLS 920 spectrometer, which employed a 300 nm line of 450 W xenon lamps as excitation source, recorded the photoluminescence (PL) emission spectra. The emission was scanned in the region of 300–700 nm. Meanwhile, the widths of both the excitation slit and the emission slit were set to 3.0 and 2.0 nm, respectively. The identity of crystalline phase of the samples was identified by the X-ray diffraction (XRD) patterns, which were obtained from a diffractometer (type DX-2500) employing Cu Kα radiation at a scan rate (2θ) of 0.05° s$^{-1}$, an accelerating voltage of 40 kV and applied current of 25 mA. It is SUPRA 55 high-resolution field emission scanning electron microscope (FE-SEM) that was used to characterize the surface morphology of the samples. X-ray photoelectron spectroscopy (Amicus) analysis was performed with a spectrometer. Charge correction was performed by referencing the C 1s peak for hydrocarbons to a binding energy of 284.8 eV. N$_2$ adsorption–desorption isotherms, which were obtained on a ASAP 2020 apparatus, of the samples to analyze the Brunauer–Emmett–Teller (BET) surface area using multipoint BET method.

## 2.3. Catalyst Test

The photocatalytic properties of pure TiO$_2$, TiO$_2$/ZnO, and Co or B doped TiO$_2$/ZnO films were evaluated by degradation of oxytetracycline (5 mg/L) or formaldehyde (5 mg/L) in an aqueous solution under visible light irradiation. Prior to our experimentation, the solution of 5 mL target pollutants in the weighing bottle and the films at the bottom of the bottle were placed in the dark for 30 min before illumination to establish adsorption-desorption equilibrium. To perform the photocatalytic reaction, the pure TiO$_2$ and modified TiO$_2$ films were exposed to a light source which was positioned over samples at the height of 15 cm. The visible light source came from a tungsten halogen lamp equipped with a UV cut-off filters (λ > 400 nm), whose the average light intensity was 40 mW/cm$^2$. UV–Vis Spectrometer (TU-1901) was adopted to assess the photo-degradation activity of the film photocatalysts. The degradation rate of organic pollutants could be calculated by the formula: $\eta = (1 - c/c_0) \times 100\%$, where $c_0$ is the initial concentration of the organic solutions, while $c$ is the final concentration after illumination. In order to detect the concentration of formaldehyde whose colorlessness caused the difficulty of detection, acetylacetone spectrophotometry was selected to determine its content because of its fewer disturbance factors, easy of operation, and good reproducibility. In our experiment, the experimental error was found to be within the acceptable limit ($\pm 5\%$).

## 3. Results and Discussion

### 3.1. Photocatalytic Activity

Oxytetracycline as an antibiotic is a representative degradation-resistant organic pollutant which can be frequently detected in wastewater, so it is essential to remove it from contaminated water before discharging it into the environment [16]. Figure 3 shows decomposition kinetics of oxytetracycline solutions using pure $TiO_2$, composite $TiO_2/ZnO$, Co doped $TiO_2/ZnO$, B doped $TiO_2/ZnO$, and Co-B codoped $TiO_2/ZnO$ films on glass substrates under visible light irradiation for 100 min. There is almost no degradation for oxytetracycline solutions using pure $TiO_2$ film as shown in Figure 3. The degradation percentage of oxytetracycline solutions using Co-B codoped $TiO_2/ZnO$ film is about 42% at the end of the test, compared with using B doped $TiO_2/ZnO$ 31%, Co doped $TiO_2/ZnO$ 26%, and $TiO_2/ZnO$ 10%, respectively.
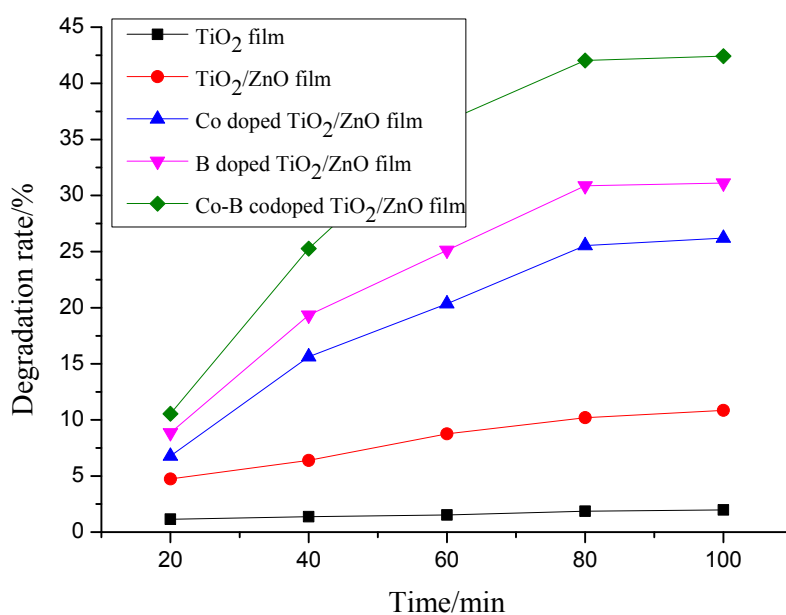


**Figure 3.** Decomposition kinetics of oxytetracycline solutions using pure $TiO_2$, composite $TiO_2/ZnO$, Co doped $TiO_2/ZnO$, B doped $TiO_2/ZnO$, and Co-B codoped $TiO_2/ZnO$ films on glass substrates under visible light irradiation for 100 min.

Formaldehyde as a carcinogen is an organic pollutants which can be also frequently detected in wastewater [17]. Figure 4 shows decomposition kinetics of formaldehyde solutions using pure $TiO_2$, composite $TiO_2/ZnO$, Co doped $TiO_2/ZnO$, B doped $TiO_2/ZnO$, and Co-B codoped $TiO_2/ZnO$ films on glass substrates under visible light irradiation for 100 min. Compared with pure $TiO_2$ film 9%, the degradation percentage of formaldehyde solutions using $TiO_2/ZnO$, Co doped $TiO_2/ZnO$, B doped $TiO_2/ZnO$, and Co-B codoped $TiO_2/ZnO$ film has reached 34%, 51%, 60% and 80%, respectively, during use time in our test. Therefore, the prepared Co-B codoped $TiO_2/ZnO$ film is effective for the decomposition of both formaldehyde and oxytetracycline solutions under visible light irradiation. The oxytetracycline solution is more difficult due to its stable naphthacene ring structure compared to the degradation for formaldehyde.

From the above experimental results, the combination of $TIO_2$ with ZnO and Co/B codoping is an effective way to improve the photocatalytic efficiency of $TiO_2$. On one hand, the slight negative shift of the ZnO band can facilitate the injection of electrons from the CB of ZnO to the CB of $TiO_2$, effectively increases the availability of $e^-$ and $h^+$ by reducing their recombination. On the other hand, Co doping can narrow the band gap and enhance the intensity of absorption in the visible region, while B ions can be mainly incorporated into metal oxide lattices acting as shallow traps for electrons

to prolong the life of the photo-generated electrons and holes. It is worth noting that the photocatalytic activity of the modified $TiO_2$ film is strongly dependent on the doped concentration since the ion doping can serve not only as a mediator of interfacial charge transfer but also as a recombination center. In our experiment, the optimal doped concentrations of Co and B ions were $7 \times 10^{-3}$ and $9 \times 10^{-2}$ mol/L, respectively.
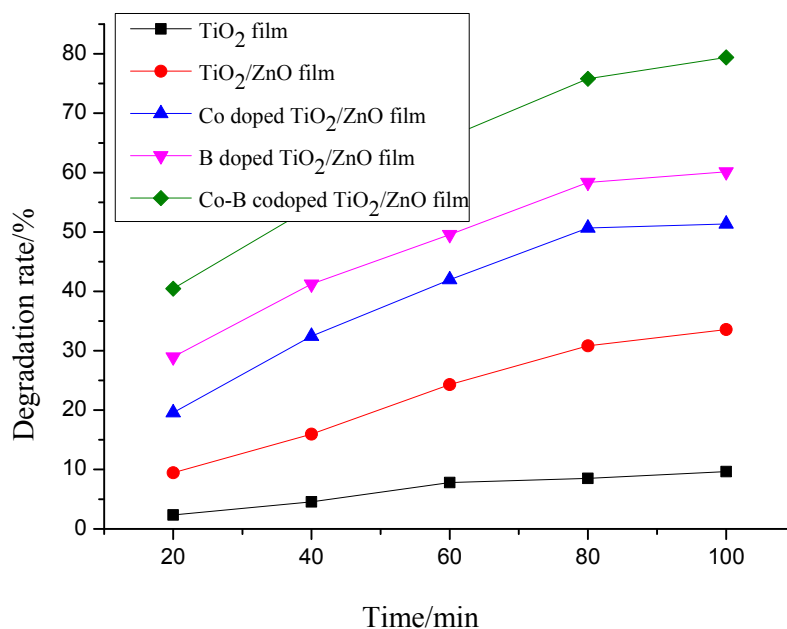


**Figure 4.** Decomposition kinetics of formaldehyde solutions using pure $TiO_2$, composite $TiO_2/ZnO$, Co doped $TiO_2/ZnO$, B doped $TiO_2/ZnO$, and Co-B codoped $TiO_2/ZnO$ films on glass substrates under visible light irradiation for 100 min.

### 3.2. Sample Characterization

3.2.1. Optical Absorption

It is band gap energy that plays vital role in enhancing spectral response to visible region of semiconductor materials. UV–Vis absorption spectra (a) and the band gap (b) of pure $TiO_2$, composite $TiO_2/ZnO$, and optimal Co-B codoped $TiO_2/ZnO$ films are depicted in Figure 5. Obviously, the Co-B codoped $TiO_2/ZnO$ film shows a red shift of the absorption edge to visible light region. The optical band gaps of a crystalline semiconductor can be calculated from the equation: $\alpha h\nu = A\ (h\nu\text{-}E_g)^{n/2}$, in which $\alpha$, $h$, $E_g$, and A are the absorption coefficient, light frequency, band gap, and a constant, respectively. The value of $n$ is determined by the type of optical transition of a semiconductor. The band gap energy of samples can be determined by extrapolation of the liner portion of the $(\alpha h\nu)^{1/2}$ versus energy ($h\nu$) curve to the energy axis [18]. The calculated energy band gaps ($E_g$) of $TiO_2$, $TiO_2/ZnO$, and Co-B codoped $TiO_2/ZnO$ films are 3.2, 2.88, and 2.06 eV, respectively. The decrease of the band gap energy is expected to be helpful for the photoactivity because more photoexcited carriers can participate in the photocatalytic reaction and their lifetime is elongated. In other words, the synergetic effects of ZnO composite and Co-B codoping can result in formation of doping level within the band gap of $TiO_2$ and thus effectively narrow the band gap.
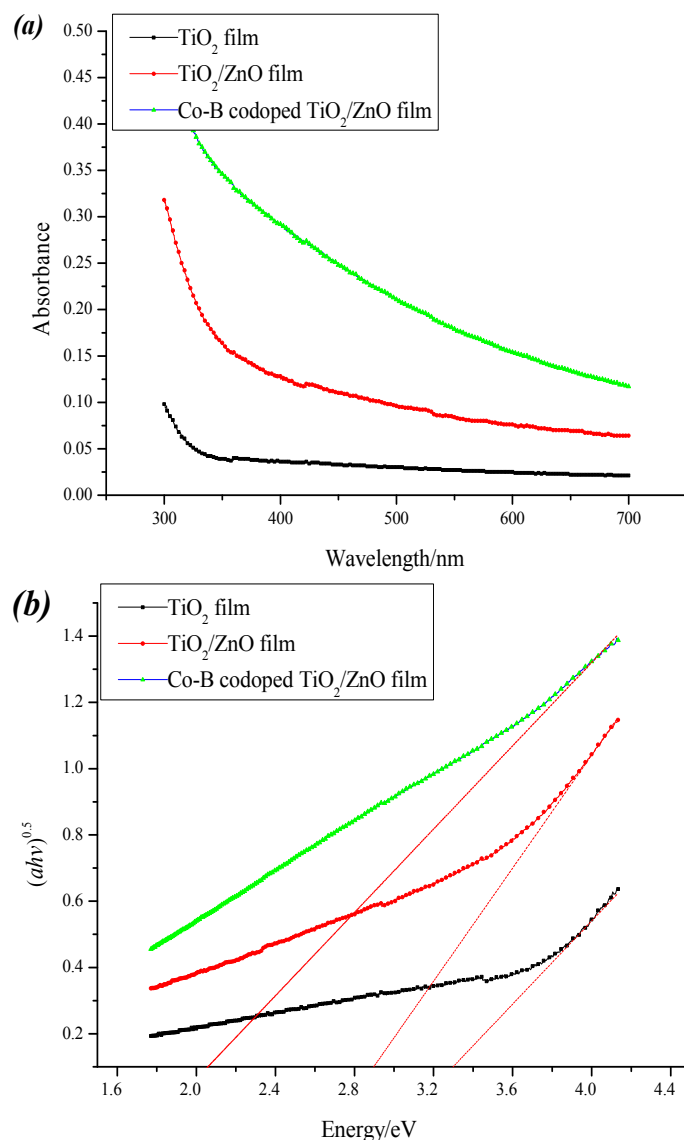
**Figure 5.** UV–Vis absorption spectra (**a**) and the band gap (**b**) of pure $TiO_2$, composite $TiO_2/ZnO$, and Co-B codoped $TiO_2/ZnO$ films.

### 3.2.2. PL Analysis

In order to further disclose the effects of ZnO coupling and Co-B codoping on the formation of photoexcited charge carriers and their recombination kinetics, PL spectra are employed to follow the lifetime of photogenerated electron-hole pairs. Figure 6 shows PL spectra of pure $TiO_2$, composite $TiO_2/ZnO$, and Co-B codoped $TiO_2/ZnO$ films. Although the peak position (about 370 nm) of the three samples is similar, their PL intensities are quite different. The PL intensity of Co-B codoped $TiO_2/ZnO$ film is the lowest compared to pure $TiO_2$ and composite $TiO_2/ZnO$, indicating the recombination of electrons and holes was effectively prohibited. The increased lifetime of the charge carriers can enhance the photocatalytic activity of Co-B codoped $TiO_2/ZnO$ film.

According to the above analyses, we can draw the conclusion that ZnO coupling and Co-B codoping can not only induce strong visible light absorption but also decrease the recombination rate of electron-hole pairs. It was also noteworthy that Co-B codoping may play a leading role for narrowing the band gap, whereas ZnO coupling may exhibit prior function in prolonging the life time of photoexcited charge carriers.
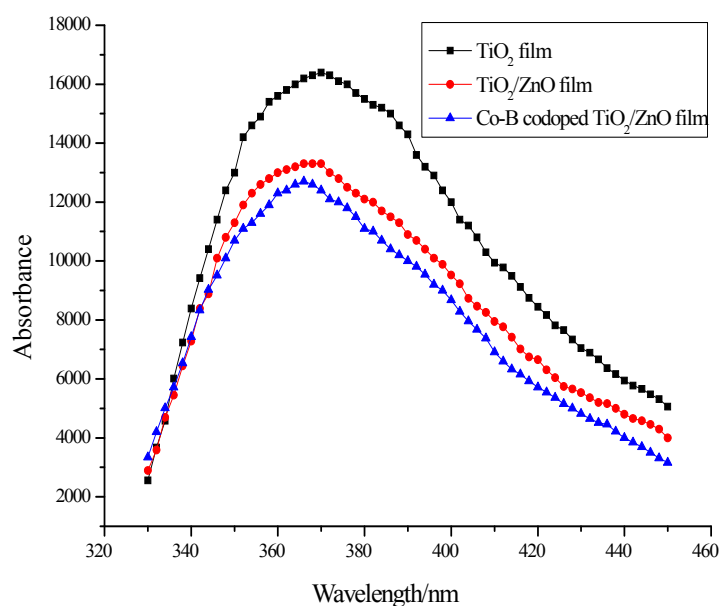
**Figure 6.** PL spectra of pure $TiO_2$, composite $TiO_2/ZnO$, and Co-B codoped $TiO_2/ZnO$ films.

### 3.2.3. Crystal Structure

Photocatalytic efficiency of semiconductor materials is strongly dependent on their crystal structure. Figure 7 presents the XRD patterns of pure $TiO_2$ and Co-B codoped $TiO_2/ZnO$ samples calcined at 450 °C in air for 1 h. From Figure 7, pure $TiO_2$ shows a mixed crystallinity composed of anatase, brookite, and rutile. The main diffraction peaks at $2\theta = 25.3°$, $37.3°$, and $48.1°$ are assigned to the (101), (004), and (200) planes of the anatase phase of $TiO_2$, respectively. The diffraction peak at $2\theta = 30.3°$ is assigned to the (121) plane of the brookite phase of $TiO_2$. The diffraction peaks at $2\theta = 27.3°$ and $36.8°$ are assigned to the (110) and (101) planes of the rutile phase of $TiO_2$. It is clear that the (101) reflections are dominant in the spectrum, well according to the standard diffraction data of $TiO_2$ powder (JCPDS No. 21-1276). Compared to the diffraction peaks of pure $TiO_2$, those of the Co-B codoped $TiO_2/ZnO$ are more broad and weak, indicating a small crystal size of this sample [3,19]. According to the Scherrer equation: $D = 0.89\lambda/\beta\cos\theta$, the average crystallite sizes of pure $TiO_2$ and Co-B codoped $TiO_2/ZnO$ are 7 and 3 nm, respectively, indicating that the multi-modification $TiO_2$ can effectively hinder the increase of the crystallite size. In addition, it can be seen that the rutile peaks almost disappear thus forming an anatase-brookite heterojunction. As the latest report, the biphase heterojunction $TiO_2$ can achieve higher photocatalytic activity than whichever single phase $TiO_2$ due to the synergistic effect between anatase and brookite [20]. The peaks of ZnO are so weak that they can be hardly observed due to two possible reasons. One is that the coupling amount of ZnO in this system is very small. The other is that the peaks of $TiO_2$ are so strong that the weak peaks of ZnO are covered [21]. Similarly, there is no Co and B related compound peaks are observed indicating that the small amounts of Co and B dopants are uniformly distributed on $TiO_2$.

### 3.2.4. Surface Morphology

As we know, the photocatalytic properties of catalysts are usually influenced by their surface morphology. Figure 8 shows FE-SEM micrographs of pure $TiO_2$ and Co-B codoped $TiO_2/ZnO$ films calcined at 450 °C in air for 1 h. Compared with pure $TiO_2$ film with cracks, the Co-B codoped $TiO_2/ZnO$ film without cracks was composed of smaller round-like nanoparticles. It is well-known that a good dispersion or reduced aggregation among particles may increase the active site, thus improving photocatalytic degradation of organic pollutants.
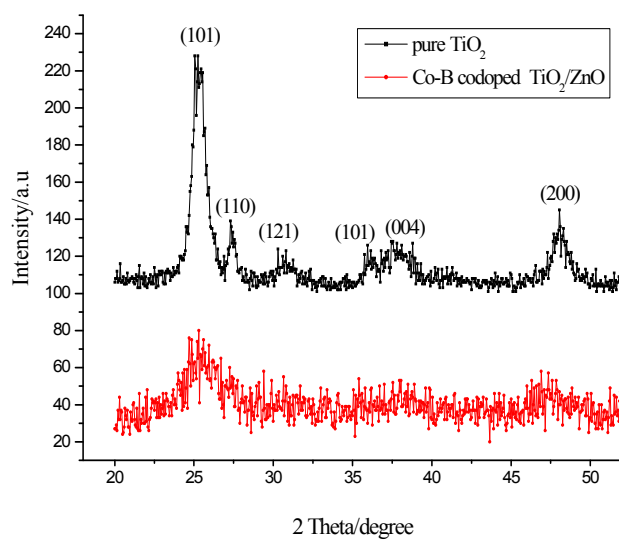
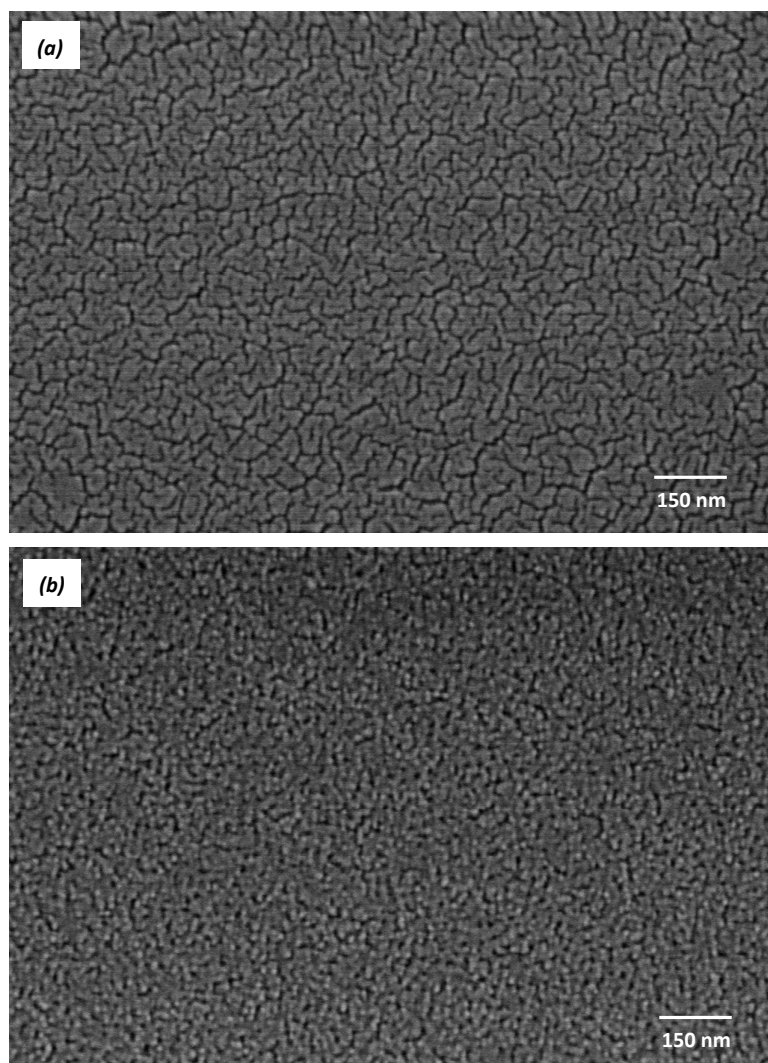**Figure 7.** XRD patterns of pure $TiO_2$ and Co-B codoped $TiO_2/ZnO$ samples.



**Figure 8.** FE-SEM images of (**a**) pure $TiO_2$ and (**b**) Co-B codoped $TiO_2/ZnO$ films.

### 3.2.5. XPS Study

X-ray photoelectron spectroscopy can be carried out to determine the surface elemental composition of the catalyst. Figure 9 shows XPS image of Co-B codoped $TiO_2$/ZnO film calcined at 450 °C for 1 h. From Figure 9, the characteristic peaks of B 1s, C 1s, Ti 2p, O 1s, Co 2p, and Zn 2p are observed with the binding energies of ~195, 285, 459, 531, 799, and 1044 eV, respectively, consistent with the values reported in literature [22,23]. The presence of C element may come from residual carbon of organic precursors used in the sol-gel method and adventitious hydrocarbon. A weak broad peak with a binding energy centered at ~195 eV is observed for the sample, indicating that the B species may mainly occupy the interstitial site of $TiO_2$. In addition, it is found that the incorporation of Co species also facilitates the formation of oxygen vacancies, which may be due to charge imbalance associated with the substitution of $Ti^{4+}$ ions. Composition analysis by energy-dispersive spectroscopy (EDS) indicates that the atomic concentrations of Ti, O, Zn, Co, B, and C in the film are 15.12, 64.90, 0.62, 0.47, 0.79, and 18.10%, respectively.
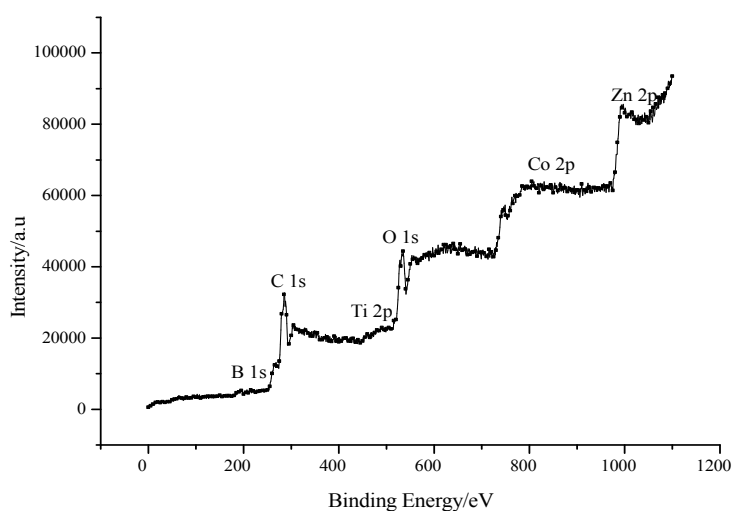


**Figure 9.** XPS image of Co-B codoped $TiO_2$/ZnO film.

### 3.2.6. Surface Areas

Specific surface areas play an important role in influencing the photocatalytic activity of $TiO_2$. Figure 10 shows $N_2$ adsorption/desorption isotherms (a) and pore size distribution (b) of pure $TiO_2$, composite $TiO_2$/ZnO, and Co-B codoped $TiO_2$/ZnO powders. From Figure 10a, the isotherms of the samples exhibit distinct hysteresis loops from 0.4 to 1.0 at high relative pressures. The distinct hysteresis loop is indicative of a bottle-neck mesoporous structure existed, possibly caused by non-uniform pore size. Compared with pure $TiO_2$ and composite $TiO_2$/ZnO, the Co-B codoped $TiO_2$/ZnO sample has largest adsorption quantities at the same relative pressure. The surface area of pure $TiO_2$, composite $TiO_2$/ZnO, and Co-B codoped $TiO_2$/ZnO are 47.8, 74.6, and 115.8 $m^2$/g, respectively. The three samples have a similar narrow pore size distribution, but their pore volumes are different as shown in Figure 10b. In our case, the pore volumes are 0.077, 0.092, and 0.104 $cm^3$/g for pure $TiO_2$, $TiO_2$/ZnO, and Co-B codoped $TiO_2$/ZnO samples, respectively. The large surface area and pore volume can effectively adsorb more $H_2O$, $O_2$, and pollutants on the reactive sites of the catalysts, thus improving the photocatalytic activity of the modified $TiO_2$.
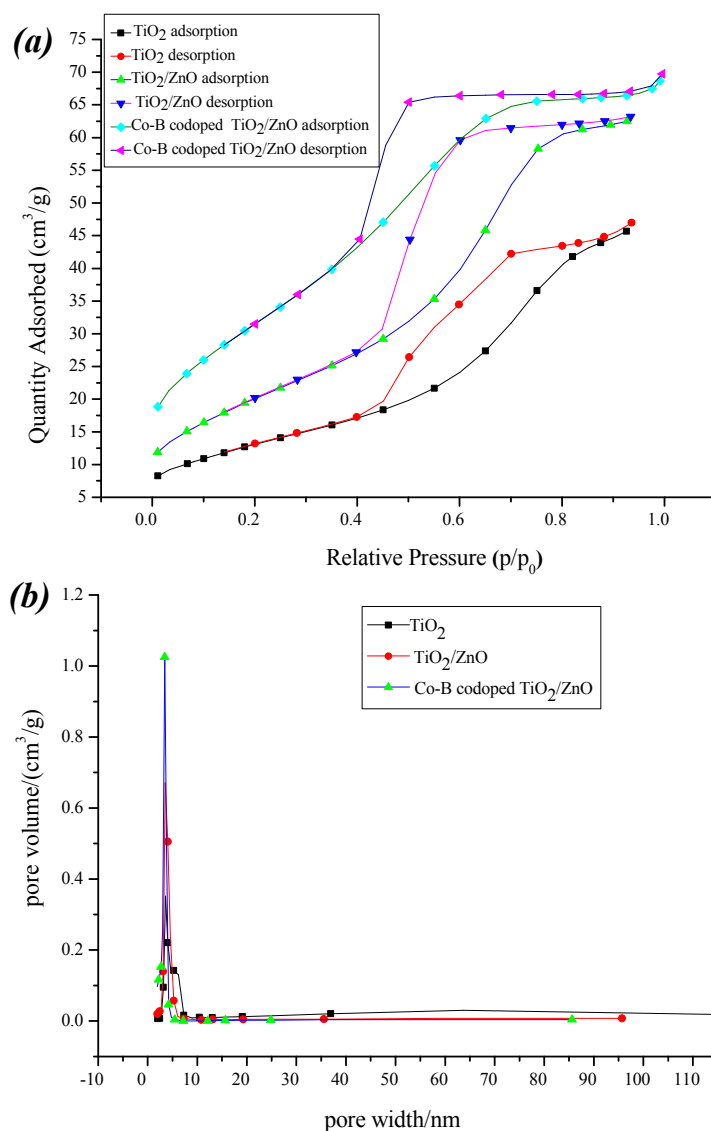
**Figure 10.** $N_2$ adsorption/desorption isotherms (**a**) and pore size distribution (**b**) of pure $TiO_2$, composite $TiO_2/ZnO$, and Co-B codoped $TiO_2/ZnO$ powders.

Based on the above experiments, the Co-B codoped $TiO_2/ZnO$ composite films exhibit excellent photocatalytic activity under visible light irradiations. According to the FE-SEM, BET, and XRD analyses, Co-B codoping and ZnO coupling can effectively lessen the aggregation of the $TiO_2$ nanoparticles, increase specific surface area of the $TiO_2$ film, and inhibit the transformation of anatase to rutile at high temperature. According to the PL and DRS spectra analyses, Co-B codoping and ZnO coupling can not only induce strong visible light absorption but also reduce the recombination rate of electron–hole pairs. These factors lead to effective photodegradation of organic pollutants.

## 4. Conclusions

In summary, the Co-B codoped $TiO_2/ZnO$ films were successfully fabricated on the surface of common glass substrates by a simple sol-gel approach and a controllable dip-coating technique. Compared with pure $TiO_2$, Co-B codoped $TiO_2/ZnO$ film showed excellent photocatalytic activity under visible light irradiation. According to PL, DRS, XRD, SEM, and BET analyses, the Co-B codoped $TiO_2/ZnO$ film with large surface area and narrowed band gap energy was composed of smaller

nanoparticles compared to pure $TiO_2$. The high photocatalytic performance and low cost of the Co-B codoped $TiO_2$/ZnO film will make it a promising material in the application of disposing wastewater.

**Author Contributions:** M.-M.Y. and M.W. conceived and designed the experiments; M.W. performed the experiments; Q.-S.L. and F.L. analyzed the data; X.-L.P. contributed reagents/materials/analysis tools; M.-M.Y. and M.W. wrote the paper; all authors have read the final version of the manuscript.

**Conflicts of Interest:** The authors declare no conflict of interest.

## References

1. Chen, C.C.; Ma, W.H.; Zhao, J.C. Semiconductor-mediated photodegradation pollutants under visible-light irradiation. *Chem. Soc. Rev.* **2010**, *39*, 4206–4219. [CrossRef] [PubMed]
2. Han, F.; Kambala, V.S.R.; Srinivasan, M.; Rajarathnam, D.; Naidu, R. Tailored titanium dioxide photocatalysts for the degradation of organic dyes in waste water treatment. *Appl. Catal. A* **2009**, *359*, 25–40. [CrossRef]
3. Kong, X.B.; Li, F.; Qi, Z.N.; Qi, L.; Yao, M.M. $SnO_2$-based thin films with excellent photocatalytic performance. *J. Mater. Sci. Mater. Electron.* **2017**, *28*, 7660–7667. [CrossRef]
4. Ahmad, R.; Mohsin, M.; Ahmad, T.; Sardar, M. Alpha amylase assisted synthesis of $TiO_2$ nanoparticles: Structural characterization and application as antibacterial agents. *J. Hazard. Mater.* **2015**, *283*, 171–177. [CrossRef] [PubMed]
5. Yao, Y.; Guan, L.X.; Ma, Y.; Yao, M.M. Ce-S codoped $TiO_2$-$SiO_2$ composite nanocrystalline film with visible light photocatalytic activity. *J. Mater. Sci. Mater. Electron.* **2017**, *28*, 3013–3019. [CrossRef]
6. Bettinelli, M.; Dallacasa, V.; Falcomer, D.; Fornasiero, P.; Gombac, V.; Montini, T.; Romano, L.; Speghini, A. Photocatalytic activity of $TiO_2$ doped with boron and vanadium. *J. Hazard. Mater.* **2007**, *146*, 529–534. [CrossRef] [PubMed]
7. Wang, D.T.; Li, X.; Chen, J.F.; Tao, X. Enhanced photoelectrocatalytic activity of reduced graphene oxide/$TiO_2$ composite films for dye degradation. *Chem. Eng. J.* **2012**, *198–199*, 547–554. [CrossRef]
8. Asahi, R.; Morikawa, T.; Ohwaki, T.; Aoki, K.; Taga, Y. Visible-light photocatalysis in nitrogen-doped titanium oxides. *Science* **2001**, *293*, 269–271. [CrossRef] [PubMed]
9. Wang, F.; Jiang, Y.; Gautam, A.; Li, Y.; Amal, R. Exploring the origin of enhanced activity and reaction pathway for photocatalytic $H_2$ production on Au/B-$TiO_2$ catalysts. *ACS Catal.* **2014**, *4*, 1451–1457. [CrossRef]
10. Lei, Y.; Zhao, G.; Liu, M.; Zhang, Z.; Tong, X.; Cao, T. Fabrication, Characterization, and Photoelectrocatalytic Application of ZnO Nanorods Grafted on Vertically Aligned $TiO_2$ Nanotubes. *J. Phys. Chem. C* **2009**, *113*, 19067–19076. [CrossRef]
11. Shen, S.J.; Yang, T.S.; Wong, M.S. Co-sputtered boron-doped titanium dioxide films as photocatalysts. *Surf. Coat. Technol.* **2016**, *303*, 184–190. [CrossRef]
12. Li, F.; Li, H.; Guan, L.X.; Yao, M.M. Nanocrystalline $Co^{2+}$/$F^-$ codoped $TiO_2$-$SiO_2$ composite films for environmental applications. *Chem. Eng. J.* **2014**, *252*, 1–10. [CrossRef]
13. Zaleska, A.; Grabowska, E.; Sobczak, J.W.; Gazda, M.; Hupka, J. Photocatalytic activity of boron-modified $TiO_2$ under visible light: The effect of boron content, calcination temperature and $TiO_2$ matrix. *Appl. Catal. B* **2009**, *89*, 469–475. [CrossRef]
14. Zhao, N.; Yao, M.M.; Li, F.; Lou, F.P. Microstructures and photocatalytic properties of $Ag^+$ and $La^{3+}$ surface codoped $TiO_2$ films prepared by sol-gel method. *J. Solid State Chem.* **2011**, *184*, 2770–2775. [CrossRef]
15. Li, H.; Zhang, W.; Guan, L.X.; Li, F.; Yao, M.M. Visible light active $TiO_2$-ZnO composite films by cerium and fluorine codoping for photo-catalytic decontamination. *Mater. Sci. Semicond. Process.* **2015**, *40*, 310–318. [CrossRef]
16. Zhao, C.; Pelaez, M.; Duan, X.D.; Deng, H.P.; O'Shea, K.; Fatta-Kassinos, D.; Dionysiou, D.D. Role of pH on photolytic and photocatalytic degradation of antibiotic oxytetracycline in aqueous solution under visible/solar light: Kinetics and mechanism studies. *Appl. Catal. B* **2013**, *134–135*, 83–92. [CrossRef]
17. Guimaraes, J.R.; Farah, C.R.T.; Maniero, M.G.; Fadini, P.S. Degradation of formaldehyde by advanced oxidation processes. *J. Environ. Manag.* **2012**, *107*, 96–101. [CrossRef] [PubMed]

18. Yan, X.D.; Zou, C.W.; Gao, X.D.; Gao, W. ZnO/TiO$_2$ core-brush nanostructure: Processing, microstructure and enhanced photocatalytic activity. *J. Mater. Chem.* **2012**, *22*, 5629–5640. [CrossRef]

19. Zheng, L.R.; Zheng, Y.H.; Chen, C.Q.; Zhan, Y.Y.; Lin, X.Y.; Zheng, Q.; Wei, K.M.; Zhu, J.T. Network Structured SnO$_2$/ZnO Heterojunction Nanocatalyst with High Photocatalytic Activity. *Inorg. Chem.* **2009**, *48*, 1819–1825. [CrossRef] [PubMed]

20. El-Sheikh, S.M.; Zhang, G.S.; El-Hosainy, H.M.; Ismail, A.A.; O'Shea, K.E.; Falaras, P.; Kontos, A.G.; Dionysiou, D.D. High performance sulfur, nitrogen and carbon doped mesoporous anatase-brookite TiO$_2$ photocatalyst for removal of microcystin-LR under visible light irradiation. *J. Hazard. Mater.* **2014**, *280*, 723–773. [CrossRef] [PubMed]

21. Seddigi, Z.S.; Bumajdad, A.; Ansari, S.P.; Ahmed, S.A.; Danish, E.Y.; Yarkandi, N.H.; Ahmed, S. Preparation and characterization of Pd doped ceria-ZnO nanocomposite catalyst for methyl tert-butyl ether (MTBE) photodegradation. *J. Hazard. Mater.* **2014**, *264*, 71–78. [CrossRef] [PubMed]

22. Wu, Y.T.; Gong, Y.Y.; Liu, J.Q.; Zhang, Z.; Xu, Y.; Ren, H.; Li, C.; Niu, L.Y. B and Y co-doped TiO$_2$ photocatalyst with enhanced photodegradation efficiency. *J. Alloy Compd.* **2017**, *695*, 1462–1469. [CrossRef]

23. Zheng, X.Z.; Li, D.Z.; Li, X.F.; Chen, J.; Cao, C.S.; Fang, J.L.; Wang, J.B.; He, Y.H.; Zheng, Y. Construction of ZnO/TiO$_2$ photonic crystal heterostructures for enhanced photocatalytic properties. *Appl. Catal. B* **2015**, *168–169*, 408–415. [CrossRef]

**Sample Availability:** Samples of the compounds are not available from the authors.